Received: 9 July 2019 | Revised: 30 September 2019 | Accepted: 27 October 2019 | Published on: 29 November 2019

DOI: 10.1002/met.1855

RESEARCH ARTICLE

Meteorological Applications RMetS

Development of upper air simulator for the calibration of solar radiation effects on radiosonde temperature sensors

Sang-Wook Lee | Inseok Yang | Byung IL Choi | Sunghun Kim | Sang-Bong Woo | Woong Kang | Youn Kyun Oh | Seongchong Park | Jae-Keun Yoo | Jong Chul Kim | Young Hee Lee | Yong-Gyoo Kim

Division of Physical Metrology, Korea Research Institute of Standards and Science (KRISS), Daejeon, South Korea

Correspondence
Yong-Gyoo Kim, Division of Physical Metrology, Korea Research Institute of Standards and Science (KRISS), Daejeon 34113, South Korea.
Email: dragon@kriss.re.kr

Funding information
Korea Evaluation Institute of Industrial Technology, Grant/Award Number: 10067387; Korea Research Institute of Standards and Science, Grant/Award Number: 19011040

Abstract

For the accurate measurement of temperature in the upper air by using radiosondes, one prerequisite is the compensation of solar radiation effects that cause sensor heating. The development at the Korea Research Institute of Standards and Science (KRISS) of an upper air simulator (UAS) that can simulate radiation effects is reported. The UAS can independently control four environmental parameters: irradiance, temperature, pressure and air speed. An entire radiosonde can be installed in the test chamber and the measurement data transmitted remotely *via* an antenna. Solar irradiance is mimicked by using a solar simulator that irradiates the radiosonde sensor. The temperature of the test chamber is controlled from −70 to 20°C by placing it inside a climatic chamber. The pressure and ventilation speed in the test chamber are modulated using combinations of sonic nozzles, a mass flow controller and a vacuum pump. A ventilation speed of 5 $m \cdot s^{-1}$, which mimics the speed of ascent of the radiosondes when lifted using a balloon, is achieved at pressures as low as 7 hPa. The capability of controlling the environmental parameters independently and the stability of each parameter are presented. As a proof of concept, the radiation-induced bias on the temperature sensor of a commercial radiosonde Vaisala RS41 is measured. The effect of each parameter is investigated by varying it while keeping the other parameters fixed. Radiosonde calibration using the UAS at the KRISS will help improve the traceability of upper air measurements to the International System of Units.

KEYWORDS

air temperature correction, calibration, radiosonde, solar irradiation, thermal metrology for climate, upper air

1 | INTRODUCTION

Measurements of air temperature and water vapour are critical for weather and climate monitoring, as well as for aviation safety. Radiosondes are widely used for upper air measurements in most meteorological agencies, research institutes and air forces, and in climatology. They are equipped with various sensors and are carried by balloons up to altitudes of approximately 35 km to measure essential climate variables (ECVs), such as air temperature, humidity, pressure, and wind speed and direction *in situ*. Thus far, there has been the consensus that radiosondes may serve as a reference for other remote-sensing techniques using light detection and ranging and satellites. In this regard, one important problem related to upper air measurements using radiosondes is the achievement of a certain level of measurement accuracy. To achieve this goal, the Global Climate Observing System (GCOS) Reference Upper Air Network (GRUAN) was established for manufacturer-independent characterization of instruments and to achieve the highest level of quality control in upper air measurements from the surface to the stratosphere. The GRUAN specifies the measurement accuracy required for ECVs in the upper air to resolve climate changes for decades (GCOS, 2007, 2013). The required accuracy for temperature measurement is 0.1 K in the troposphere and 0.2 K in the stratosphere.

According to the *Guide to Meteorological Instruments and Methods of Observation* (2010) of the World Meteorological Organization (WMO), temperature measurements made using radiosondes are significantly influenced by solar radiation and long wave infrared radiation. In the latest WMO intercomparison of high-quality radiosonde systems, the correction for daytime soundings ranged from 0.6 to 2.3 K at 10 hPa, depending on the manufacturer (Nash *et al*., 2011). Some practical methods to reduce radiation-induced errors have been suggested, for example, by using small temperature sensors, coating sensor surfaces with low-absorption materials such as thin metallic layers, and minimizing thermal conduction along the electrical connections to the temperature sensor. However, a detailed methodology for calibrating radiosonde sensors to compensate for the radiation-induced warm bias has not been specified by the WMO. Only the stability requirements for temperature, pressure and humidity in the calibration apparatus have been specified. An environmental simulation chamber called the World Calibration Facility for Ozone Sondes has been established as part of the Global Atmosphere Watch Program of the WMO. Several intercomparison experiments (Jülich Ozone Sonde Intercomparison Experiment) have been conducted to assess the performance of the major types of ozone sondes (Smit and Kley, 1998). Currently, most radiosonde users rely on the radiation-effect corrections provided by manufactures. Although the temperature stability of calibration set-ups specified in the WMO guide ($\pm 0.25\ \mathrm{K{\cdot}min^{-1}}$) can be achieved down to -80°C by using commercially available climate chambers, simultaneous control of temperature, humidity and pressure in the range that is likely to be encountered in actual radiosonde soundings remains challenging. In the lower stratosphere, the solar irradiance, temperature and pressure typically encountered by radiosondes are 1,300 $\mathrm{W{\cdot}m^{-1}}$, -70°C and 10 hPa, respectively. In addition to the required stability of these parameters, the effect of ventilation on temperature sensors should be considered in the compensation of radiation effects. Ventilation may occur because of a combination of wind vectors during the ascent at a speed of approximately 5 $\mathrm{m{\cdot}s^{-1}}$, as well as from the pendulum and rotating motions of radiosondes during sounding. Previously, it was demonstrated that the increase in temperature of radiosonde sensors under irradiation was significantly reduced by ventilation (Lee *et al*., 2018a). Recently, it has been demonstrated that sensor diameter and air flow can significantly affect the radiation-induced errors of temperature sensors (de Podesta *et al*., 2018). Therefore, the construction of calibration facilities that can control all the relevant parameters simultaneously is highly desirable for achieving proper compensation of radiation-induced errors in temperature measurements.

Studies have been undertaken to compensate for the radiative errors of radiosonde temperature sensors by using chambers to control some of the environmental parameters simultaneously. In the GRUAN, the correction of solar radiation effects on a commercially available radiosonde Vaisala RS92 was studied (Dirksen *et al*., 2014). Pressure, ventilation and solar irradiance were controlled independently in a test chamber by using a vacuum pump, circulating fan, and solar simulator or natural sunlight, respectively. However, the uncertainty in ventilation speed (about 1 $\mathrm{m{\cdot}s^{-1}}$) was thought to be high compared with the typical ascent speed (5 $\mathrm{m{\cdot}s^{-1}}$), and the test temperature was limited to ambient temperature. The effects of ventilation, temperature and pressure on the correction of radiative errors have been studied separately at the Korea Research Institute of Standards and Science (KRISS) by using two independent set-ups (Lee *et al*., 2018a, 2018b, 2018c). These studies found that each parameter significantly influences the correction of warm-biased temperature under irradiation. Therefore, it is essential to construct a combined calibration facility that can help study the effects of all environmental parameters simultaneously to achieve proper correction of radiative errors in radiosonde sensors.

The present paper reports the development of an upper air simulator (UAS) that controls temperature (T), pressure (P), air ventilation (v) and irradiance (S) in the calibration of radiosonde sensors. First, the principle for controlling each parameter in the UAS is explained in detail. The temperature in the UAS is controlled using a climate chamber down to -70°C. The sonic nozzle technique is adopted to control the ventilation speed up to

6.5 m·s^{-1}, even at pressures as low as 7 hPa. Solar irradiance is mimicked using a solar simulator equipped with a xenon lamp. A cold dry-gas-generation system is attached to the UAS to control the temperature and frost-point temperature of the inlet gas down to −70 and −95°C, respectively. Second, the effect of each parameter on the temperature sensor of the commercially available radiosonde Vaisala RS41 is investigated. The sensitivity of each parameter (P, T and v) on the temperature rise due to solar radiation is evaluated, and the results are discussed. The UAS developed in the present study is expected to be able to characterize sensors for upper air measurements, which would improve the reliability of radiosonde measurements.

2 | CONSTRUCTION OF THE UAS

2.1 | Layout of the UAS

Figure 1 shows the UAS developed in this study. The UAS consists of several parts for controlling irradiance, temperature, pressure and ventilation speed simultaneously. Gas flows from the dry-gas generator, through a mass flow controller, sonic nozzles, a thermostatic bath, a test chamber and then a vacuum pump. For calibration, an entire radiosonde is installed in the test chamber, and its temperature is determined by controlling the temperature inside the climate chamber. To control the irradiance, a solar simulator is positioned outside the climate chamber. Irradiation from this simulator is transmitted through two quartz windows (left inset of Figure 1) and guided toward the radiosonde sensor in the test chamber. To control the ventilation speed at low pressures, combinations of the mass flow controller, sonic nozzles and vacuum pump are used. The dry-gas generator is used to ensure that the dew- or frost-point temperature of the input gas remains lower than the temperature of the test chamber to prevent the formation of dew or frost on the quartz windows. The temperature of the dry input gas is then adjusted to the target temperature of the test chamber by using a heat exchanger in the thermostatic bath (upper right inset of Figure 1). Detailed operation schemes of each component are described below.

2.2 | Temperature measurement

Ten type E thermocouples are used to measure the spatial distribution and temporal stability of temperature in the climate chamber. A data logger (Keysight, Model 34970A) reads the temperatures recorded by the thermocouples with internal electrical reference junction compensation. Thermocouples from the same batch are very regular, cheap and convenient for data acquisition, which makes them useful for measuring and controlling the temperature at multiple spots. A PT100 thermometer

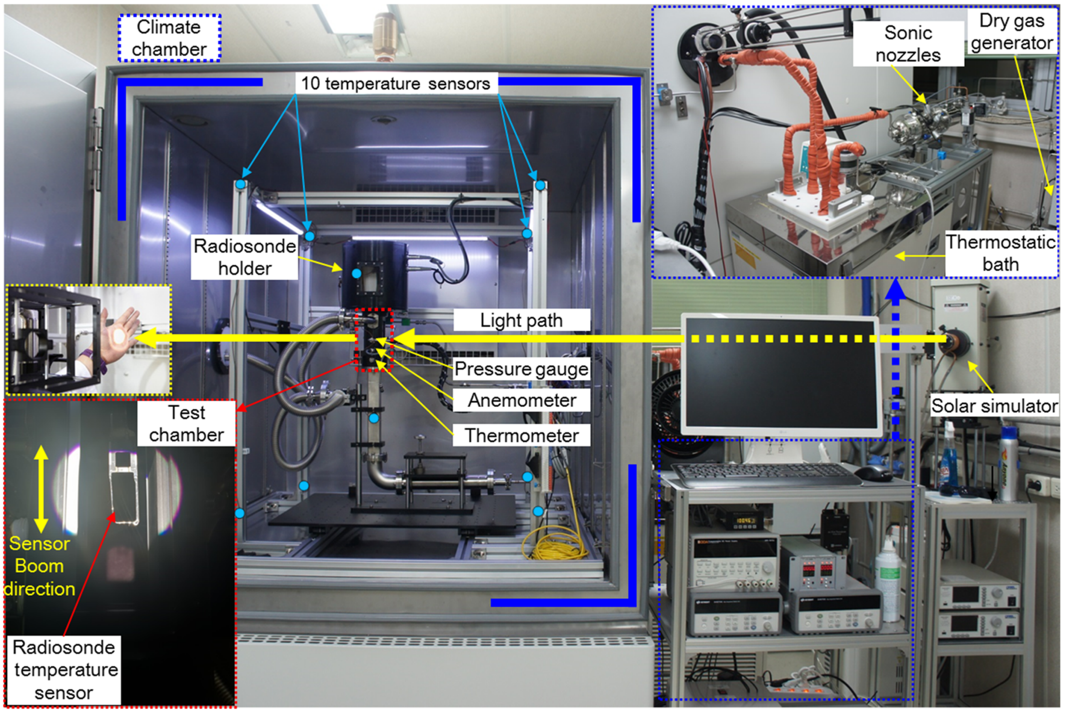

FIGURE 1 Layout of the upper air simulator (UAS)

(platinum resistance thermometer with a nominal resistance of 100 Ω at 0°C) measures the reference temperature near the radiosonde in the test chamber. Another PT100 thermometer measures the temperature at the input port of the sonic nozzle. This measurement is required in order to calculate the mass flow rate in the sonic nozzle system and, subsequently, the ventilation speed in the test chamber, as explained below. The two PT100 thermometers are read using a separate data logger (Keysight, Model 34970A).

The two PT100 thermometers are calibrated by comparison in liquid baths against calibrated standard platinum resistance thermometers as reference thermometers. The calibration uncertainty of both PT100 thermometers is 0.05°C with a coverage factor of $k = 2$.

2.3 | Generation of dry gas

The UAS operates in the temperature range of −70 to 30°C. Therefore, dry gas with a frost-point temperature < −70°C is required to prevent the formation of dew or ice on any surface. It is especially important to keep the quartz windows clear to irradiate the radiosonde sensors in the test chamber in a stable manner. Therefore, a dry-gas-generation system consisting of desiccants and a gas purifier is constructed. As illustrated in Figure 2a, compressed air passes sequentially through a water separator, desiccants and the gas purifier. As for the desiccants, six desiccant chambers with four molecular sieves and two silica gels are connected in series. After passing through the desiccant chambers, the compressed air is dried to the frost-point temperature of approximately −60°C. This gas is further dried in the gas purifier (Michell, Model PSD4-HPO) below the frost-point temperature of −95°C (about 38 nmol·mol^{-1}). The operating range of the gas purifier is 30 L·min^{-1} in terms of flow rate and up to 8,000 hPa in terms of pressure. After passing through the sonic nozzles, which control the speed and pressure of the air flow, the temperature of the dry gas is adjusted to that of the test chamber in advance by using a heat exchanger placed in a thermostatic bath (Figure 2b). The dry gas is then allowed to flow to the test chamber. The dry-gas line is branched off before it enters the sonic nozzles and is cooled using a heat exchanger in the climate chamber. The cooled dry gas is sprayed onto the quartz windows of the test chamber from the outside and onto the window of the climate chamber from the inside to prevent the formation of dew or frost and, thus, to facilitate stable light transmission.

Although the UAS currently uses dry air (frost point of −95°C), it is devised potentially to control the humidity of the test chamber by using a water vapour saturator installed in the thermostatic bath. After dry air passes through the sonic nozzles, it can be diverted into the saturator. The saturator generates a well-defined water vapour pressure in the input gas according to the temperature and pressure in the saturator (Greenspan, 1976; Hardy, 1998; Choi *et al.*, 2015). Although the saturator is not used in the current study, the UAS can potentially control the humidity in the test chamber by using the saturator in the thermostatic bath. The potential operation scheme for humidity control in the UAS test chamber was described in a recent report in which a two-temperature, two-pressure humidity generator was used for humidity generation and its validation at low temperatures and low pressures (Lee *et al.*, 2019).

2.4 | Control of air flow speed and pressure

To mimic the ascent speed of radiosondes, which is up to approximately 5 m·s^{-1} in the vertical direction, sonic nozzles are used to control the air flow rate inside the test chamber accurately. A sonic nozzle, also called a critical flow venturi, is a flowmeter with a constant-curvature convergent section to a minimum cross-section area

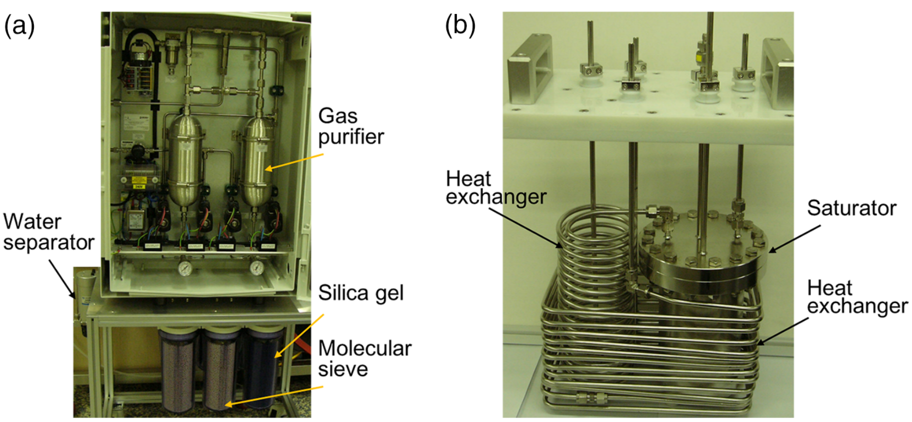

FIGURE 2 (a) Dry-gas-generation system; and (b) heat exchanger to adjust the temperature of the gas input to the test chamber temperature and the saturator for humidity control in the upper air simulator (UAS)

(i.e. throat) at which sonic conditions exist, and this section is followed by a conical divergent section (Figure 3a) (ISO-9300, 2005; ASME-MFC-7, 2016). The diameter d of a sonic nozzle is selected on the basis of the mass flow rate required for generating an air ventilation speed close to 5 m·s^{-1} in the test chamber at pressures as low as 7 hPa. The maximum constant flow of a given sonic nozzle is determined by the given up- and downstream conditions, especially by the ratio of downstream pressure (P_e) to upstream pressure (P_0). At a certain critical ratio ($[P_e = P_C]/P_0$), air speed reaches sonic conditions at the throat (Figure 3b, iii). This condition is called the choked or sonic flow state. In the sonic flow state, a constant mass flow is generated, and this mass flow is unaffected by downstream flow disturbances or pressure fluctuations so long as the pressure ratio (P_e/P_0) remains lower than the critical pressure ratio indicated by iii–vi in Figure 3c. The mass flow rate $\dot{m}$ generated by a sonic nozzle system is expressed as follows (ISO-9300, 2005; ASME-MFC-7, 2016):

$$\dot{m} = \frac{C_d C^* A P_0}{\sqrt{R T_0}} \tag{1}$$

where C_d is the sonic nozzle discharge co-efficient; C^* the gas critical flow function; A is the throat area of the sonic nozzle; R is the specific gas constant; and P_0 and T_0 are the upstream stagnation pressure and temperature, respectively. The gas critical flow function and the specific gas constant can be determined from the composition of the experimental air. The throat area of each sonic nozzle can be calculated using its diameter (d). The discharge co-efficient of a sonic nozzle can be obtained through its calibration using a low-pressure gas-flow standard system, such as the bell prover systems at the KRISS (Choi *et al.*, 2010). Therefore, once the downstream pressure is adequately low and air flows in the choked state, information about the upstream pressure and temperature is needed to determine the mass flow rate when using the sonic nozzle system. The ventilation speed inside the test chamber is then calculated using the air density determined from the temperature, pressure and cross-sectional area of the test chamber. Notably, the cross-sectional profile of air flow is assumed to be uniform in this work. The effective flow speed at the position of the radiosonde temperature sensor can differ depending on the cross-sectional profile of air flow.

Figure 4a shows the sonic nozzle system installed in the UAS. The pressure and temperature sensors are installed upstream of the sonic nozzles to calculate the mass flow rate. Pressure is measured at 1D upstream of the throat of the sonic nozzles following the international standard (where D is pipe diameter) (ISO-9300, 2005). The measurement range of the pressure sensor (Mensor, CPT6100) is from 0 to 7,000 hPa, with an uncertainty of U = 40 Pa (k = 2). The temperature sensor (GHM PT 100 Ω) with U = 0.05°C (k = 2) is installed 2D upstream

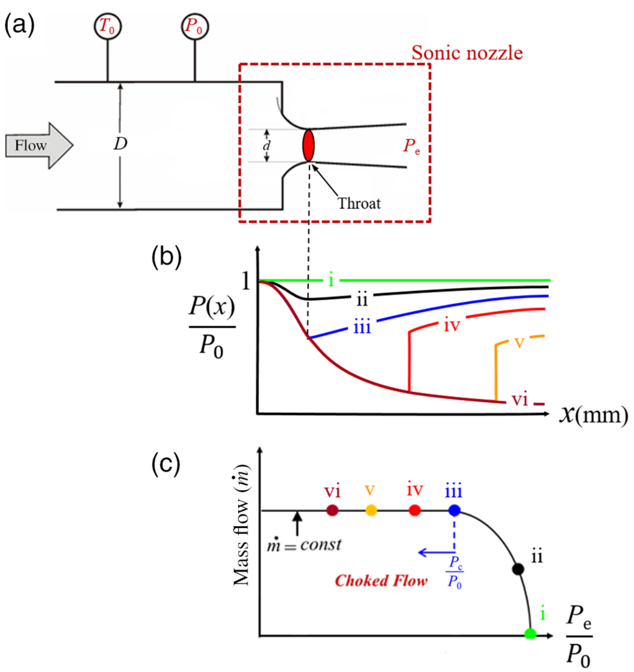

FIGURE 3 (a) Configuration of a sonic nozzle; (b) pressure distributions; and (c) mass flow rate with different up- and downstream pressures

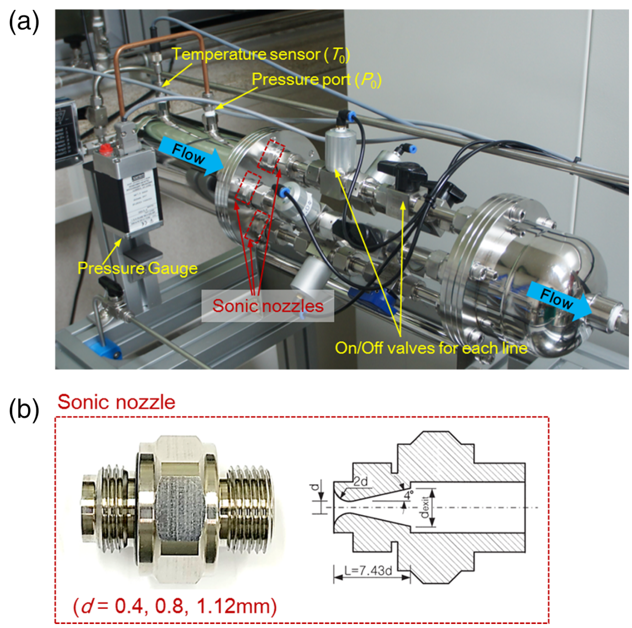

FIGURE 4 (a) Installation set-up of the sonic nozzle system for the upper air simulator (UAS); and (b) outer view and schematic diagram of a sonic nozzle

of the sonic nozzles, as recommended by the international standard. The sonic nozzles are manufactured as toroidal-throat Venturi nozzle types compliant with ISO 9300. The diameters of the three sonic nozzles used in this study are 0.4, 0.8 and 1.12 mm (Figure 4b), and their mass flow rates range from 0.06 to 0.2, from 0.2 to 0.6 and from 0.6 to 1.3 g·s^{-1}, respectively. The uncertainty of the sonic nozzles is $U = 0.18\%$ ($k = 2$), as determined from the results of a calibration conducted using a bell prover and the low-pressure gas flow standard system at the KRISS ($U = 0.13\%$, $k = 2$) (Choi *et al.*, 2010). Three calibrated sonic nozzles are installed in each pipeline with an on–off valve to allow gas flow through them depending on the required mass flow rate. Dry gas from the dry-gas-generation system is supplied to the sonic nozzles through the control valves suitably. The measured values of P_0 and T_0 upstream of the sonic nozzles can be used to determine the mass flow rate by applying Equation 1 and, subsequently, the air flow speed in the test chamber can be calculated. In the present experiments, P_0 of the sonic nozzles ranges from 2,000 to 6,000 hPa, and the downstream pressure (P_e), which is the that in the test chamber housing the radiosonde, ranges from 7 to 100 hPa. The ratio of down- to upstream pressure is adequately smaller than the critical pressure ratio for choked flow. Therefore, the sonic nozzle system in the UAS can generate a constant mass flow rate. Note that the mass flow rate is converted to the ventilation speed in the test chamber by using the air density calculated from the temperatures and pressures measured in the test chamber.

Figure 5 shows an example of the generation of constant air flow in the test chamber set to 7 hPa and −70°C. To generate the air flow speed of 5 m·s^{-1} under these conditions, the upstream pressure is controlled using the valves located between the sonic nozzles and the dry-gas generator. Figure 5a shows the stability of the pressure and temperature measurements upstream of the sonic nozzle. The resulting stability of air flow speed in the test chamber is shown in Figure 5b. The mass flow rate required to generate the air flow speed of 5 m·s^{-1} differs depending on the air density inside the test chamber. When the target temperature and pressure in the test chamber are decided, a sonic nozzle is selected to generate the desired mass flow rate with controlled upstream pressure and temperature. In all temperature and pressure ranges in the test chamber, the stability of the pressure upstream of the sonic nozzles and air flow speed in the test chamber are similar to those in the case shown in Figure 5.

2.5 | Solar irradiation system

Figure 6 shows a schematic diagram of the irradiation set-up used to apply sunlight-like irradiation to the radiosonde temperature sensor in the test chamber. A dimmable 1 kW xenon dc arc lamp (Newport, 66926-1000XF-R07) as virtual sunlight is imaged through a condenser lens set in a ϕ5 mm liquid light guide with a length of 1 m (Newport, 77636). The light is then delivered to a field lens. Finally, the field lens images the uniformly irradiating circular end of the light guide into a ϕ60 mm circular spot and then into the test chamber housing the radiosonde. Irradiance at the temperature sensor position can be varied from 0 to 1,500 W·m^{-2} by adjusting the dc-arc current.

To prevent frosting of the quartz windows, two types of air-purging systems are used. A cold purging system is installed inside the climate chamber; it blows dry gas around the inner surfaces (chamber side) and outer surfaces of the two quartz windows on the test chamber. The temperature of the supplied air is preconditioned to the working temperature of the climate chamber. The

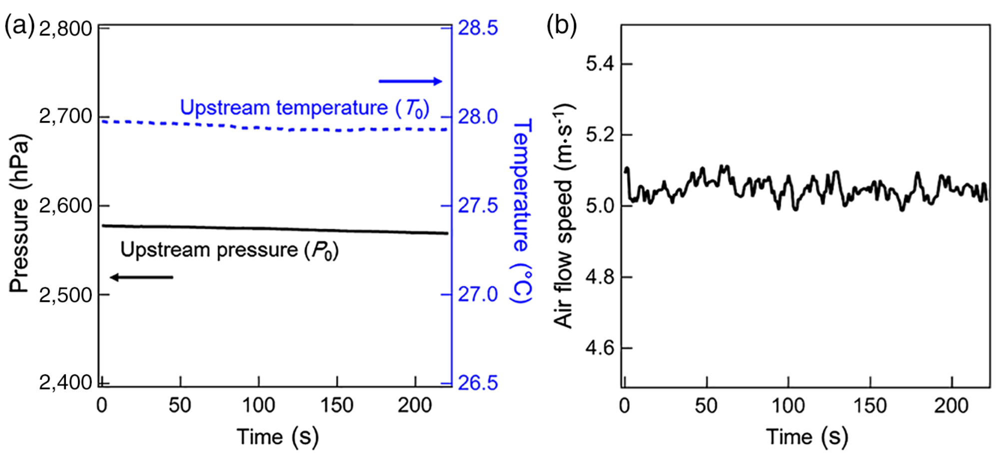

FIGURE 5 (a) Upstream pressure (P_0) and temperature (T_0) of sonic nozzles for the generation of (b) choked air flow in the test chamber (downstream) at the ventilation speed of 5 m·s^{-1} at 7 hPa and −70°C

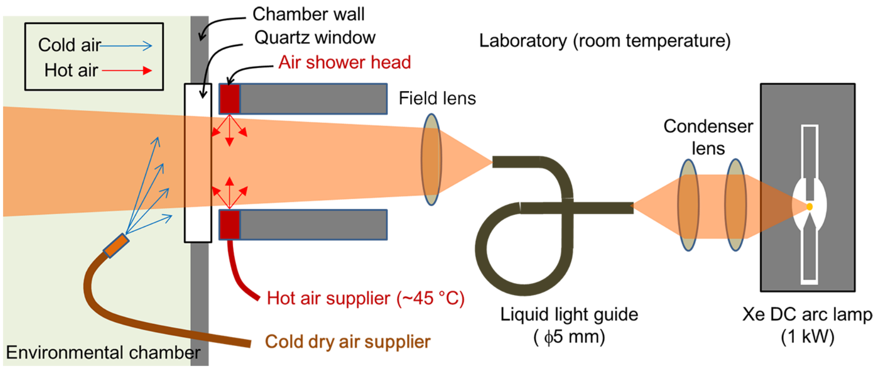

FIGURE 6 Schematic diagram of the virtual sunlight irradiation set-up (not to scale)

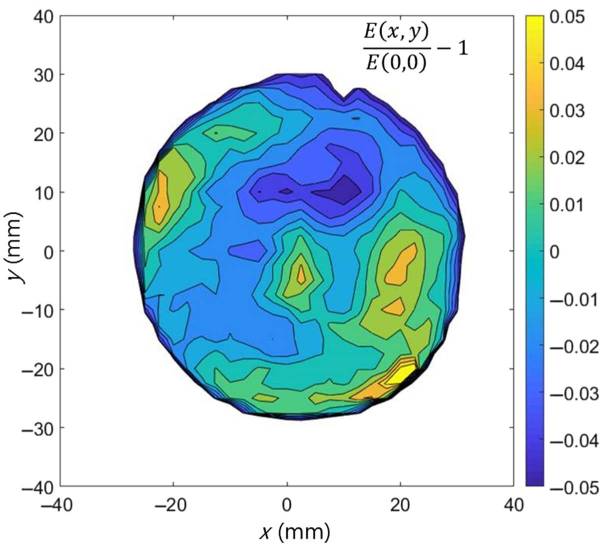

FIGURE 7 Uniformity of irradiation at the sensor-mounting position, where the irradiance at the centre (E[0,0]) is 1,300 W·m^{-2}

other purging system is a hot air system maintained at approximately 45°C; it is installed outside the climate chamber to dry the outer surface (room-side) of the quartz window.

The spatial distribution of irradiance $E(x, y)$ is measured at the radiosonde mounting position by moving the test chamber using a motor-controlled two-axis translator and a 0.8 mm^2 Si photodiode (Thorlabs, SM05PD2A). Figure 7 shows a mapping of $E(x, y)$ relative to the irradiance $E(0, 0)$ measured at the centre (1,300 W·m^{-2}). The uniformity of irradiation is ±5% within a circular area of diameter 60 mm. This measurement is used as the reference irradiance. To monitor irradiance levels during operation, a photodiode-based pyranometer (Apogee, SP-110-SS) is permanently installed behind the test chamber inside the thermostatic chamber. The pyranometer was calibrated using a thermopile-based pyranometer (Kipp & Zonen, CM-21) under the same irradiation conditions at the KRISS.

3 | RESULTS AND DISCUSSION

3.1 | Installation of Vaisala RS41

As a proof of concept of calibration using the UAS, the magnitude of solar radiation effects on a commercial radiosonde (Vaisala RS41) was investigated in the test chamber. The test chamber has two quartz windows to allow the transmission of light from the solar simulator into the test chamber and the transmission of light outward from the test chamber. The irradiation direction was perpendicular to the direction of the sensor boom (the lower left inset in Figure 1), and the irradiation area was adjustable. In this study, the irradiation area was a circle measuring 60 mm in diameter, which covered the entire temperature sensor and the area around it in the sensor boom. After passing through the sonic nozzle, air flowed into the test chamber in a direction parallel to the sensor boom. Temperature measurement data from the RS41 temperature sensor inside the test chamber were obtained remotely in the same manner as that in actual soundings using the Vaisala MW41 sounding system. The measured data consisted of raw temperature readings without radiation correction. The UAS system can be used in the wired and wireless modes, and the use of these modes is not limited to the calibration of specific radiosonde models.

3.2 | Characterization of the UAS

To investigate the effect of each environmental parameter on the compensation of radiation effects, one parameter of the UAS was systematically varied while keeping the others fixed. As an exception, only irradiance was fixed at S = 900 W·m^{-2} throughout the study because the linearity between the temperature rise of the sensors and irradiance, independently of the other parameters, has been documented in the literature (Lee *et al.*, 2018a, 2018c). In these reports, the other parameters were found to affect only the co-efficient of proportionality between the temperature rise and irradiance.

The experimental conditions in this study were as follows: temperature of the test chamber $T = -70$, -55, -40, -20, 0 and 20°C; and pressure of the test chamber $P = 7$, 10, 30, 60 and 100 hPa. The ventilation speed (v) was, for the most part, fixed to 5 m·s^{-1}, but it was varied between 4.0 and 6.5 m·s^{-1} under a few selected conditions to determine the effect of v. Notably, each parameter could be controlled independently, and, thus, the UAS was capable of generating any combination of S, T, P and v.

The calibration of a Vaisala RS41 temperature sensor at each S, T, P and v took approximately 5 min, which was the time required to operate the off, on and off states of irradiation sequentially. The stability of irradiance, represented by its standard deviation (σ) during this period, was 2.4 W·m^{-2} (0.27% of the irradiance). The reference temperature in the test chamber during the calibration time period was measured using a calibrated PT100 thermometer under varying P. The reference temperature sensor was located in a shaded region inside the test chamber. The stability of the reference temperature was $\sigma = 0.02$ K, which was deemed adequate to resolve the temperature rise of radiosonde sensors under irradiation because the temperature rise was ≥ 0.1 K (Figure 9).

The stability of P was measured in the test chamber at $T \approx -70$°C. The pressure gauge used in this study was calibrated at the KRISS before it was installed; its maximum uncertainty was $U = 45$ Pa ($k = 2$). The pressure gauge was located outside the climate chamber and connected to the test chamber *via* stainless-steel tubing. The stability of the reference air pressure, measured in terms of the relative standard deviation of the measured pressure, was < 1% over the entire pressure range. This demonstrated the stability of pressure control at both the inlet and outlet of the sonic nozzle employed in this study. Notably, the temperature inside the laboratory was controlled to 23 ± 2°C; the temperature dependence of the pressure gauge was 0.01%·°C^{-1}, suggesting that the temperature-dependent pressure fluctuation was only 0.04%.

The stability of v inside the test chamber was measured under varying P. Ventilation mimics the speed of ascent of radiosondes in a balloon, and, therefore, it was maintained at 5 m·s^{-1}, unless mentioned otherwise. The stability of v was within $\sigma = 0.03$ m·s^{-1} under all pressures. It should be noted that v was not measured but calculated based on the mass flow rate determined using Equation 1. This ventilation speed and its profile in the test chamber will be confirmed by an independent measurement using laser Doppler velocimetry.

The measurement range, stability and uncertainty of the UAS are summarized in Table 1. Notably, the uncertainty evaluation of each parameter of the UAS is preliminary. The uncertainties of temperature and pressure include factors related to sensor calibration, reproducibility, stability, digital multimeter (DMM) calibration and DMM stability. The uncertainty in irradiance can be ascribed to the calibration of the photodiode, as well as its stability and uniformity. The uncertainty in ventilation speed can be ascribed to the cross-sectional profile of air flow by assuming a maximum difference of 30% between the uniform profile (used in this study) and a parabolic profile (found in realistic scenarios). The uncertainty budget for each parameter of the UAS is preliminary and will be analysed in more detail in future.

3.3 | Effects of pressure and temperature

Figure 8 shows an example of the temperature rise of the Vaisala RS41 sensor as a function of time when the irradiation ($S = 900$ W·m^{-2}) is turned on at 38 s and turned off at 160 s with $T = -70$°C, $P = 7$ hPa and $v = 5$ m·s^{-1}. The temperature rise due to irradiation was defined as ΔT_{rad}. Figure 9 shows the effect of T (from -70 to 20°C) and P (from 7 to 100 hPa) in the test chamber on ΔT_{rad}. At $P = 100$ hPa, the effect of T on ΔT_{rad} is negligible. However, ΔT_{rad} shows a T dependence at lower pressures. It was found that ΔT_{rad} decreased gradually as T increased. ΔT_{rad} decreased by approximately 0.15°C between $T = -70$ and 20°C. This observation can possibly be ascribed to the fact that the long wave (infrared) radiation from the sensor at -70°C was smaller than that at 20°C, even though the radiation from the solar simulator was constant. In terms of convective cooling, the density, thermal conductivity and viscosity of air were found to decrease at low temperatures. Although these factors have contrary effects, one or two factors may dominate the convective cooling process at low temperatures and low pressures. In addition, the heated sensor boom or

TABLE 1 Measurement range, stability and preliminary uncertainty of the upper air simulator (UAS)

Parameter	Measurement range	Stability	Preliminary uncertainty ($k = 1$)
Temperature	−70 to 20°C	0.020°C	0.037°C
Pressure	0.7–100 hPa	0.07 hPa	0.52 hPa
Irradiance	0–1,300 W·m^{-1}	0.27%	3.10%
Ventilation speed	0–6.5 m·s^{-1}	0.03 m·s^{-1}	0.87 m·s^{-1}

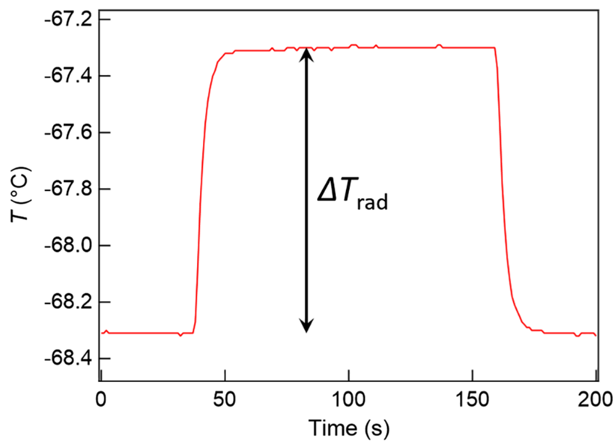

FIGURE 8 Change in temperature of RS41 due to irradiation when $T = -70°\text{C}$ and $P = 7$ hPa

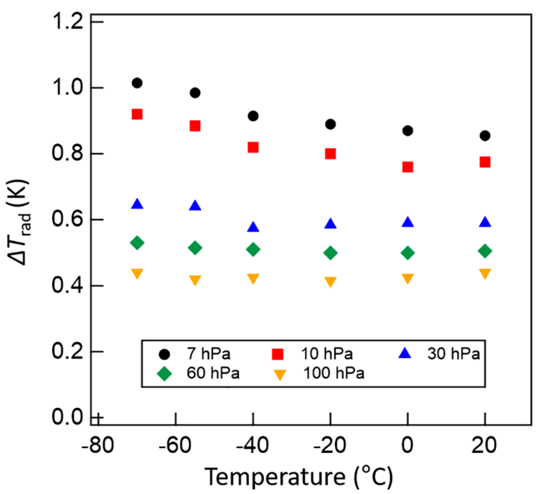

FIGURE 9 Temperature rise of the RS41 sensor due to irradiance $S = 900$ W·m^{-2} at varying temperatures from −70 to 20°C and varying pressure from 7 to 100 hPa under $v = 5$ m·s^{-1}

humidity sensor may be a significant heat source by way of thermal conduction through the sensor boom material and lead wires. The effectiveness of cooling, in turn, may vary with absolute temperature because temperature-dependent thermal conductivity in the boundary layer limits heat transfer to the surroundings. However, the T dependence was not clearly visible at pressures > 100 hPa because convectional cooling of the sensor by air flow played a dominant role in the thermal exchange process of the sensor under high P. In this regard, the effect of temperature may play a role in the compensation of radiation effects in the stratosphere, where $P < 100$ hPa but T is increased.

As shown in Figure 9, the effect of pressure on ΔT_{rad} was significant at both 20 and −70°C. Convectional cooling of the heated sensor decreased under low P because air density decreased even as the magnitude of irradiation from the solar simulator remained unchanged. Under $T = -70°\text{C}$ and $v = 5$ m·s^{-1}, ΔT_{rad} was 0.4°C at $P = 100$ hPa, but ΔT_{rad} increased to 0.9°C at $P = 10$ hPa. Therefore, ΔT_{rad} increased by more than a factor of 2 between the two cases. The combination of T and P in the former (−70°C and 100 hPa) and the latter (−70°C and 10 hPa) cases can be encountered in actual radiosonde soundings depending on altitude, latitude and season. Therefore, the formula to compensate for the effects of solar radiation on radiosonde sensors should not simply be a function of altitude or pressure but one of multiple environmental parameters, including temperature and ventilation speed.

The operational radiation correction of the Vaisala RS41 is a function of pressure and solar angle, but not of temperature (Vaisala). Although the assumptions and conditions for radiation correction in case of the UAS are different from those in the case of Vaisala, the two sets of conditions and assumptions are broadly compared in Table 2. Since the correction value of the UAS was obtained at 900 W·m^{-1}, it is grown by the ratio (1,360/900 W·m^{-1}) of the realistic solar irradiance in the stratosphere to the experimental irradiance. In general, the radiation correction of the UAS is slightly higher (0.1–0.2°C) than the operational radiation correction. In this study, all experiments were performed with a fixed direction of the sensor boom, which was set perpendicular to the irradiance and parallel to the air flow. In this position, the effect of S and v can be over- and underestimated, respectively. Currently, a new test chamber that permits adjustment of the sensor boom angle has been designed and is under construction. Radiation correction of the UAS by using the new test chamber is expected to be lower than the current values.

3.4 | Effect of ventilation speed

Finally, the effect of v was investigated by varying it from 4.0 to 6.5 m·s^{-1} in the test chamber. This v range was selected to simulate variations in the speed of ascent of radiosondes by balloon. Ventilation speed affects convectional cooling of the sensor heated by radiation. Thus, ΔT_{rad} decreases as v increases (Figure 10). The effect of ventilation seemed to be slightly enhanced at −55°C compared with that at 0°C. This observation was ascribed to the temperature effect described above. Nevertheless, the effect of v on ΔT_{rad} was only of the order of 0.04°C/(m·s^{-1}).

In a previous study, Dirksen *et al.* (2014) employed the following empirical model for Vaisala RS92:

$$\triangle T = a \cdot \left(\frac{I}{p \cdot v}\right)^{\text{b}} \tag{2}$$

TABLE 2 Radiation corrections of the Vaisala RS41 and upper air simulator (UAS)

	Operational radiation correction of the Vaisala RS41; ventilation speed of 6 m·s^{-1}		Radiation correction of the UAS; irradiation angle of 90° to the sensor boom; ventilation speed of 5 m·s^{-1}; and irradiance of 1,360 W·m^{-1}	
Pressure (hPa)	Solar angle 45°	Solar angle 90°	Temperature −40°C	Temperature −70°C
100	0.42°C	0.45°C	0.63°C	0.65°C
60	–	–	0.78°C	0.81°C
50	0.58°C	0.62°C	–	–
10	1.10°C	1.16°C	1.23°C	1.38°C
7	–	–	1.38°C	1.53°C
5	1.39°C	1.45°C		–

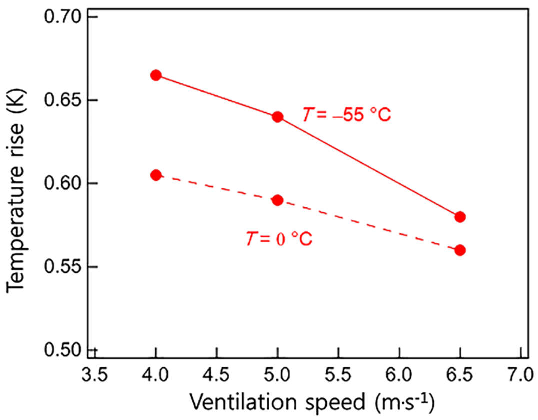

FIGURE 10 Temperature rise of the RS41 sensor due to irradiance $S = 900$ W·m^{-2} at varying ventilation speeds of 4.0, 5.0 and 6.5 m·s^{-1} at −55°C (solid line) and 0°C (dashed line) at $P = 30$ hPa

where $\triangle T$ denotes the correction value; I is irradiance; P is pressure; v is ventilation speed; and a (0.18) and b (0.55) are empirical co-efficients. According to this model, the ratio of radiation errors at ventilation speeds of 4.0–6.5 m·s^{-1} should be approximately 1.31 in Figure 10. However, the ratios are 1.16 and 1.10 at −55 and 0°C, respectively. This discrepancy can possibly be ascribed to the fact that different ventilation speeds were used in the two studies. The above model was developed at ventilation speeds of 2.5 and 5 m·s^{-1}, and at these speeds, the effect of ventilation is stronger than that in the ventilation speed range of 4.0–6.5 m·s^{-1}. In addition, data scattering from the model was identified as another possible cause of the discrepancy.

4 | CONCLUSIONS

In this study, an upper air simulator (UAS), which is capable of independently controlling temperature, pressure, ventilation and irradiance, was developed, and the calibration of the Vaisala RS41 sensor was demonstrated in the UAS by compensating for the effects of radiation. The UAS employs sonic nozzles to generate air flow speeds of up to 6.5 m·s^{-1}, even at pressures as low as $P \approx 7$ hPa. By taking advantage of the unique characteristics of sonic nozzles for stabilizing downstream pressures and air flow speeds, the stability of T, P and v in the test chamber were found to be 0.02°C, 0.07 hPa and 0.03 m·s^{-1}, respectively.

The effects of T, P and v were investigated individually by varying each parameter independently in the UAS while keeping the others fixed. At low temperatures, ΔT_{rad} of the sensor upon exposure to solar irradiance increased, suggesting the effect of absolute temperature on radiation correction. The effects of both P and v were responsible for the convective cooling of sensors. Therefore, ΔT_{rad} increased as P and v decreased.

The application of radiation correction by using the UAS to actual soundings will be useful only when uncertainty evaluation of the laboratory measurements is completed. For calculation of the uncertainty of radiation correction, a model relating all parameters is required so that the uncertainty of each parameter propagates through it. A previous report by Dirksen *et al.* (2014) on the Vaisala RS92 was based on an empirical model and the corresponding uncertainty evaluation. In this regard, modelling of the radiation correction and the corresponding uncertainty evaluation of the UAS measurements are the foremost topics for future work.

In this study, by using the UAS, the individual effects of each environmental parameter on the compensation of solar radiation effects for the RS41 have been presented uniquely. On the basis of the UAS measurements, a quasi-theoretical correction formula governing heat transfer of the sensor can be developed with empirically obtainable co-efficients. However, the current version of the test chamber only allows irradiation in the direction perpendicular to the sensor boom and ventilation in the direction parallel to the sensor boom. With this fixed direction, the effects of S and v may be over- and underestimated, respectively. To mitigate this problem, a revised test chamber that allows rotation of the radiosonde around the vertical axis (the direction of the sensor boom) has been designed and is under construction. Moreover, the revised chamber will allow bending of the sensor boom from the position aligned with the vertical axis to change the angles of irradiation and ventilation with respect to the radiosonde. The effect of solar elevation angle and rotating motion of radiosondes can then be included in the correction formula for, and uncertainty evaluation of, radiation effects in future.

ACKNOWLEDGEMENT

This work was supported by the Korea Research Institute of Standards and Science (KRISS) under the project 'Establishment of National Physical Measurement Standards and Improvements of Calibration/Measurement Capability' (grant number 19011040). This paper is partly based on the work supported by the Ministry of Trade, Industry & Energy (MOTIE) of Korea under Industrial Technology Innovation Program No. 10067387 'High Speed and High Precision Radiosonde'.

ORCID

Sang-Wook Lee https://orcid.org/0000-0002-2425-6380
Inseok Yang https://orcid.org/0000-0001-7945-9671

REFERENCES

ASME-MFC-7. (2016) Measurement of gas flow by means of critical flow venturis and critical flow nozzles. In: *The American Society of Mechanical Engineers*. Washington, DC: ASME.

Choi, H.M., Park, K.-A., Oh, Y.K. and Choi, Y.M. (2010) Uncertainty evaluation procedure and intercomparison of bell provers as a calibration system for gas flow meters. *Flow Measurement and Instrumentation*, 21, 488–496.

Choi, B., Lee, S.-W., Kim, J. and Woo, S. (2015) Extension of humidity standards to −105°C frost point. *International Journal of Thermophysics*, 36, 2231–2241.

Dirksen, R., Sommer, M., Immler, F., Hurst, D., Kivi, R. and Vömel, H. (2014) Reference quality upper-air measurements: GRUAN data processing for the Vaisala RS92 radiosonde. *Atmospheric Measurement Techniques*, 7, 4463–4490.

GCOS. (2007) GCOS REFERENCE UPPER-AIR NETWORK (GRUAN): Justification, requirements, siting and instrumentation options.

GCOS. (2013) The GCOS Reference Upper-Air Network (GRUAN) GUIDE.

Greenspan, L. (1976) Functional equations for the enhancement factors for CO_2-free moist air. *Journal of Research of the National Bureau of Standards–A. Physics and Chemistry*, 80, 41–44.

Hardy, B. (1998) ITS-90 formulations for vapor pressure, frostpoint temperature, dewpoint temperature, and enhancement factors in the range–100 to+ 100 C. *Proceedings of the Third International symposium on humidity and moisture, Teddington, London, England.*

ISO-9300. (2005) Measurement of gas flow by measurement of critical flow Venturi nozzles, International Standard.

Lee, S.W., Park, E.U., Choi, B.I., Kim, J.C., Woo, S.B., Kang, W., Park, S., Yang, S.G. and Kim, Y.G. (2018a) Compensation of solar radiation and ventilation effects on the temperature measurement of radiosondes using dual thermistors. *Meteorological Applications*, 25, 209–216.

Lee, S.W., Park, E.U., Choi, B.I., Kim, J.C., Woo, S.B., Park, S., Yang, S.G. and Kim, Y.G. (2018b) Correction of solar irradiation effects on air temperature measurement using a dual-thermistor radiosonde at low temperature and low pressure. *Meteorological Applications*, 25, 283–291.

Lee, S.W., Park, E.U., Choi, B.I., Kim, J.C., Woo, S.B., Park, S., Yang, S.G. and Kim, Y.G. (2018c) Dual temperature sensors with different emissivities in radiosondes for the compensation of solar irradiation effects with varying air pressure. *Meteorological Applications*, 25, 49–55.

Lee, S.-W., Choi, B.I., Woo, S.-B., Kim, J.C. and Kim, Y.-G. (2019) Development of a low-temperature low-pressure humidity chamber for calibration of radiosonde humidity sensors. *Metrologia*, 56, 025009.

Nash, J., Oakley, T., Vömel, H. and Li, W. (2011) *WMO Intercomparisons of High Quality Radiosonde Systems*. Geneva, Switzerland: WMO, 12 July–3 August 2010.

de Podesta, M., Bell, S. and Underwood, R. (2018) Air temperature sensors: dependence of radiative errors on sensor diameter in precision metrology and meteorology. *Metrologia*, 55, 229–244.

Smit, H.G. and Kley, D. (1998) JOSIE: The 1996 WMO International intercomparison of ozonesondes under quasi flight conditions in the environmental simulation chamber at Jülich. *Proceedings of the XVIII Quadrennial Ozone Symposium*, L'Aquila, Italy: Parco Scientifico e Tecnologici d'Abruzzo, pp 971–4.

Vaisala, Vaisala Radiosonde RS41 Measurement Performance. Available at: https://www.vaisala.com/sites/default/files/documents/WEA-MET-RS41-Performance-White-paper-B211356EN-B-LOW-v3.pdf [Accessed 15th November 2019].

WMO. (2010) Guide to meteorological instruments and methods of observation. Chapter 12. Measurement of upper-air pressure, temperature and humidity WMO-No. 8. Available at: https://library.wmo.int/doc_num.php?explnum_id=3158 [Accessed 15th November 2019].

How to cite this article: Lee S-W, Yang I, Choi BIL, *et al.* Development of upper air simulator for the calibration of solar radiation effects on radiosonde temperature sensors. *Meteorol Appl*. 2020;27:e1855. https://doi.org/10.1002/met.1855